1 **Oral Hsp90 inhibitor, SNX-5422, attenuates SARS-CoV-2 replication and dampens**

2 **inflammation in airway cells.**

3

4 Title character count: 107/150

5

6 Ria Goswami[1,5], Veronica S. Russell[1#], Joshua J. Tu[1], Philip Hughes[2], Francine Kelly[3],

7 Stephanie N. Langel[1,5], Justin Steppe[1], Scott M. Palmer[3], Timothy Haystead[2], Maria Blasi[1,4]*

8 and Sallie R. Permar[1,5*¥€].

9

10 [1]Duke Human Vaccine Institute, Duke University Medical Center, Durham, North Carolina, USA.

11 [2]Department of Pharmacology and Cancer Biology, Duke University Medical Center, Durham,

12 North Carolina, USA.

13 [3]Division of Pulmonary, Allergy and Critical Care Medicine, Department of Medicine, Duke

14 University Medical Center, Durham, North Carolina, USA.

15 [4]Division of Infectious Diseases, Department of Medicine, Duke University Medical Center,

16 Durham, North Carolina, USA.

17 [5]Department of Pediatrics, Duke University Medical Center, Durham, North Carolina, USA.

18

19 # Present address: Computational Biology and Bioinformatics, Duke University School of

20 Medicine, Durham, North Carolina, USA.

21 ¥ Present address: Department of Pediatrics, Weill Cornell Medicine, New York, USA.

22

23 *Correspondence: maria.blasi@duke.edu and sap4017@med.cornell.edu

24 €Lead contact: sap4017@med.cornell.edu

25

26

SUMMARY

Currently available SARS-CoV-2 therapeutics are targeted towards moderately to severely ill patients and require intravenous infusions, with limited options for exposed or infected patients with no or mild symptoms. While vaccines have demonstrated protective efficacy, vaccine hesitancy and logistical distribution challenges will delay their ability to end the pandemic. Hence, there is a need for rapidly translatable, easy-to-administer-therapeutics, that can prevent SARS-CoV-2 disease progression, when administered in the early stages of infection. We demonstrate that an orally bioavailable Hsp90 inhibitor, SNX-5422, currently in clinical trials as an anti-cancer therapeutic, inhibits SARS-CoV-2 replication *in vitro* at a high selectivity index. SNX-5422 treatment of human primary airway epithelial cells dampened expression of inflammatory pathways associated with poor SARS-CoV-2 disease outcomes. Additionally, SNX-5422 interrupted expression of host factors that are crucial for SARS-CoV-2 replication machinery. Development of SNX-5422 as SARS-CoV-2-early-therapy will dampen disease severity, resulting in better clinical outcomes and reduced hospitalizations.

Word count: 149/150

KEYWORDS.

COVID-19, SARS-CoV-2, Hsp90, Post-exposure prophylaxis, anti-inflammatory, host-directed therapy, orally bioavailable.

INTRODUCTION.

Since its emergence in 2019, severe acute respiratory syndrome coronavirus 2 (SARS-CoV-2) rapidly spread worldwide and the disease associated with SARS-CoV-2 infection, Coronavirus

2

53   disease 2019 (COVID-19), was declared a pandemic by the WHO in March 2020 (Cucinotta and

54   Vanelli, 2020). As of February 9th, 2021, there were more than 106 million confirmed infections

55   and >2.3 million deaths, worldwide (WHO Coronavirus Disease (COVID-19) Dashboard, 2020),

56   making this ongoing disease the deadliest pandemic of the 21st century. Clinical manifestations

57   of SARS-CoV-2 infection can range from asymptomatic (Nishiura et al., 2020) and mild upper

58   airway symptoms to severe lower respiratory complications such as pneumonia, acute

59   respiratory distress syndrome (ARDS), and multi-organ system dysfunction (Huang et al.,

60   2020a), leading to respiratory compromise (Giamarellos-Bourboulis et al., 2020) and death

61   (Mehraeen et al., 2020).

62

63   There is an ongoing effort to characterize SARS-CoV-2 pathogenesis and identify prophylactic

64   and therapeutic approaches to suppress COVID-19 severity and improve clinical outcomes.

65   Currently used treatment modalities for SARS-CoV-2 infection include repurposed small

66   molecules such as remdesivir (Beigel et al., 2020), immunomodulatory agents such as

67   corticosteroids (Prescott and Rice, 2020), and virus-specific monoclonal antibodies (Zhou

68   et al., 2020b). However, most of these treatment strategies require intravenous infusions,

69   and are administered in moderately to severely ill patients. Moreover, while prophylactic

70   vaccines for SARS-CoV-2 infection have demonstrated robust protection, vaccine hesitancy

71   and logistical distribution challenges, especially in low-to-middle income countries (LMIC),

72   will restrict their ability to quickly end the global pandemic. Thus, there remains an urgent

73   need for rapidly translatable post-exposure prophylactic interventions that can be

74   administered during the early course of infection to prevent severe disease outcomes,

75   hospitalizations, and reduce viral transmissions. Since such interventions will be

76   administered to patients with no-to-mild symptoms, these therapies should be easy to store

77   and administer, and have a wide margin of safety.

78

79   Cellular chaperone protein heat shock protein 90 (Hsp90), in addition to maintaining

80   cellular homeostasis (Zhao and Houry, 2005, Taipale et al., 2010), also facilitates proper

81   folding and functionality of virally encoded proteins (Geller et al., 2007). Hence, Hsp90

82   serves as host determinant for a wide diversity of viruses (Geller et al., 2012, Rathore et

83   al., 2014, Smith and Haystead, 2017), including Coronaviruses (CoVs) such as severe

84   acute respiratory syndrome coronavirus (SARS-CoV) (Li et al., 2004, Li et al., 2020),

85   Middle east respiratory syndrome coronavirus (MERS-CoV) (Li et al., 2020) and SARS-

86   CoV-2 (Emanuel et al., 2020, Li et al., 2020). Recent *in silico* studies have proposed Hsp90

87   as a potential anti-SARS-CoV-2 target (Iyad et al., 2020). Furthermore, in a murine model

88   of sepsis, Hsp90 inhibition has been associated with dampened systemic and pulmonary

89   inflammation and acute lung injury (ALI) (Chatterjee et al., 2007), the key phenomena

90   associated with poor SARS-CoV-2 clinical outcomes (Bussani et al., 2020, Pandolfi et al.,

91   2020, Blanco-Melo et al., 2020). Hence, a trial was launched to test the efficacy of

92   intravenously administered Hsp90 inhibitor, ganetespib (ADX-1612) against SARS-CoV-2

93   infection (Aldeyra Therapeutics Press Release, 2020).

94

95   SNX-5422 is an orally bioavailable Hsp90 inhibitor (Fadden et al., 2010, Huang et al., 2009),

96   which is currently in clinical trials for solid state malignancies and lymphomas. The toxicity

97   profile of this small molecule has been extensively characterized in humans, and found to be

98   very well tolerated with no reported adverse effects or evidence of immunosuppression (Infante

99   et al., 2014, Rajan et al., 2011). Since Hsp90 can be exploited by viruses for their replication,

100   here, we have evaluated the efficacy of SNX-5422 as a post-exposure prophylactic

101   treatment for SARS-CoV-2 infection and have mapped the interaction of the drug with

102   primary human airway cell transcriptional profile. Our data reveal that SNX-5422, added

103   shortly after infection, suppresses *in vitro* SARS-CoV-2 replication with a high selectivity index,

104   and influences expression of cellular genes associated with SARS-CoV-2 replication and poor

105   disease outcomes, including airway inflammatory pathways. Our findings support further

106   development of SNX-5422 as an oral post-exposure therapeutic for SARS-CoV-2 infection

107   that will reduce the length of viral infectivity and dampen virus-associated inflammatory

108   responses, initiated early in the course of infection. A post-exposure therapy geared

109   towards individuals in the initial phase of infection, will reduce COVID-19 disease severity

110   and hospitalizations and will prevent additional global deaths, while the distribution of

111   prophylactic vaccines ramps up.

112

113   **RESULTS AND DISCUSSION.**

114

115   **SNX-5422, an orally bioavailable Hsp90 inhibitor, is a potent suppressor of SARS-**

116   **CoV-2 replication.**

117

118   Recent *in silico* drug repositioning studies and single-cell transcriptomic analysis have

119   identified Hsp90 as a host dependency factor for SARS-CoV-2 replication (Iyad et al., 2020,

120   Emanuel et al., 2020). Inhibition of Hsp90 was associated with suppression of SARS-CoV-2

121   replication *in vitro* (Emanuel et al., 2020, Li et al., 2020, Kamel et al., 2020). Here, we

122   sought to determine if an orally bioavailable, highly selective inhibitor of Hsp90 (SNX-5422)

123   (Okawa et al., 2009), currently in clinical trials for cancer therapy (Infante et al., 2014,

124   Rajan et al., 2011), could serve as a post-exposure prophylactic or early therapeutic for

125   SARS-CoV-2 infection. To mimic post-exposure prophylaxis *in vitro*, human lung epithelial

126   cells (Calu-3), and African green monkey kidney cells (Vero E6) (Ogando et al., 2020) were

127   incubated with SARS-CoV-2 strain USA-WA1/2020 for 1hr, and the virus-exposed cells

128   were treated with increasing doses of SNX-5422 or DMSO (drug-vehicle). Using

129   immunostaining and fluorescent imaging of virus-infected Vero E6 cells, we first assessed

130   the antiviral activity of SNX-5422 by comparing proportion of viral nucleocapsid (NP)

131   protein positive cells in drug-treated vs. vehicle-treated cells. Our data indicate that SNX-

132   5422 attenuated intracellular NP expression (Figure 1A) and proportion of NP+ cells

133   (Figure 1B) in a dose dependent manner, with a 50% inhibitory concentration (IC50) of

134   2.3µM (Table 1). We further evaluated the antiviral activity of a dose range of SNX-5422 by

135   comparing viral RNA shedding in cell supernatants of drug-treated vs. vehicle-treated Vero

136   cells and human lung epithelial cells. SNX-5422 treatment resulted in a reduction of cell-

137   free viral genomic copies (Figure 1C and 1D) with an IC50 of 0.2µM in both cell types

138   (Table 1). Additionally, SNX-5422-treatment reduced cell-free infectious viral titers (Figure

139   1E and 1F) with an IC50 of 0.38µM in Vero E6 cells and 0.4µM in Calu-3 cells (Table 1).

140

141   Since SNX-5422 inhibits the functionality of Hsp90, (Fadden et al., 2010, Huang et al.,

142   2009), a host chaperone necessary for maintaining cellular homeostasis (Zhao and Houry,

143   2005, Taipale et al., 2010), we determined the selectivity index of the drug in inhibiting

144   SARS-CoV-2 replication. Uninfected Vero E6 and Calu-3 cells were treated with increasing

145   concentrations of SNX-5422 and the frequency of live cells was monitored by flow

146   cytometry (Figure 1G and 1H). The 50% cellular cytotoxicity (CC50) of SNX-5422 was

147   computed to be 91.97µM and >100µM in Vero E6 and Calu-3 cells, respectively,

148   highlighting the minimal cytotoxic effects of the drug on these two cell types. Consequently,

149   the selectivity index (SI=CC50/IC50) of SNX-5422 in suppressing viral replication was

150   evaluated to be high in both cell types (Table 1). Collectively, these data suggest that

151   treatment with an oral inhibitor of Hsp90, SNX5422, upon SARS-CoV-2 exposure, can

152   potently attenuate viral replication *in vitro*, at a high selectivity index.

153

154   **SNX-5422 treatment of primary human tracheobronchial epithelial (TBE) cells alters**

155   **expression of cellular inflammatory and metabolic pathways.**

156

6

157   In addition to developing antivirals targeting specific viral proteins, there has been a

158   growing effort in developing therapeutics targeting host proteins exploited by viruses for

159   their replication or implicated in viral pathogenesis (Nitulescu et al., 2020). As such

160   therapeutics can impair normal functioning of host proteins, a clear understanding of their

161   impact on cellular mechanisms is critically important. We therefore characterized the

162   interactions of SNX-5422 with the cellular machinery using a physiologically relevant *ex*

163   *vivo* human primary tracheobronchial epithelial (TBE) cell model (Mason, 2020). Fully

164   differentiated human TBE cells from three independent donors (Table S1) without known

165   respiratory disease or smoking history were cultured *ex vivo* at the air-liquid interface. The

166   basolateral side of the cell culture was treated with either 0.1% DMSO (drug-vehicle) or

167   1µM SNX-5422 for 48hrs, followed by bulk RNA sequencing of the total cellular RNA

168   (Figure 2A). Principal component analysis of the read counts revealed that treatment with

169   SNX-5422 formed distinct clusters compared to the control group (Figure S1), highlighting

170   differential expression of cellular genes upon drug treatment. Differentially expressed

171   genes (DEGs) between the control group and the SNX-5422-treated group were defined as

172   protein coding genes with a Log_2 fold change (FC) ratio > 2 and adjusted p value ≤ 0.001. A

173   volcano plot of the protein coding genes indicated that 1361 genes were differentially

174   expressed between the two groups, with 470 cellular genes being upregulated and 891

175   cellular genes being downregulated upon SNX-5422 treatment (Figure 2B). To identify

176   cellular genes whose expression was highly regulated upon SNX-5422 treatment of TBE

177   cells, we collated DEGs with a Log_2 FC >6, for which the average normalized read count

178   across donors and experimental conditions was ≥300 (Table S2). Using this stringent

179   threshold, we identified 16 cellular genes that were downregulated and 4 cellular genes

180   that were upregulated upon drug treatment (Figure 2B). Further categorization of those

181   genes based on functions revealed that SNX-5422-treatment of TBE cells downregulated

182   cytokines and chemokines that serve as chemoattractant for lymphocytes and neutrophils

183 (*CCL20, CXCL1*), regulators of cellular inflammation (*CSF3, S100A8*) and proliferation

184 *(CDC20)*, antigen presentation pathway-associated genes (*HLA-DOA, HLA-DMB*) and

185 genes functioning as solute transporters (*SLC13A2, SLC26A4, SLC5A1, SLC5A5*) (Figure

186 2B).

187

188 Next, we mapped the cellular signaling pathways that were significantly altered upon SNX-

189 5422 treatment of human TBE cells, by performing a Kyoto Encyclopedia of Genes and

190 Genomes (KEGG) pathway overrepresentation analysis on the DEGs (Figure 2C and 2D).

191 Notably, cellular inflammatory pathways such as IL-17 signaling pathway, cytokine-cytokine

192 receptor interaction, TNF-signaling pathway, Th17 cell differentiation, NOD-like receptor

193 signaling and chemokine signaling pathways were among the top 20 identified pathways

194 that were downregulated by SNX-5422 treatment. In addition, signaling pathways

195 associated with regulation of cell cycle and cellular senescence, and metabolic pathways

196 such as biosynthesis of amino acids and tryptophan metabolism, were also downregulated

197 by SNX-5422 (Figure 2C). Furthermore, treatment with this oral Hsp90 inhibitor resulted in

198 upregulation of key cellular pathways involved in physiological functions such as cellular-

199 adhesion, regulation of apoptosis and cellular proliferation (Figure 2D). Taken together, our

200 data suggest that SNX-5422 alters TBE cell inflammation, cellular proliferation, and

201 metabolism.

202

203 **SNX-5422 dampens cellular inflammatory pathways associated with SARS-CoV-2**

204 **replication and poor disease prognosis.**

205

206 SARS-CoV-2 infection has been associated with hyper-induction of pro-inflammatory

207 cytokines resulting in multiple organ failure, ALI and ARDS (Song et al., 2020).

208 Interestingly, Hsp90 inhibition dampened systemic and pulmonary inflammation and lung

209   injury in a murine model of sepsis (Chatterjee et al., 2007). Since SNX-5422 exhibited

210   downregulated inflammatory transcriptomic pathways in human TBE cells, we interrogated

211   whether these pathways have been previously associated with SARS-CoV-2 disease

212   progression. To this end, we first selected a gene set whose expression was stringently

213   regulated upon SNX-5422 treatment of human TBE cells (Log$_2$ FC >3, total 287 genes)

214   (Table S2). We then performed an extensive literature search in PubMed and non-peer

215   reviewed pre-publication repositories to compare our identified gene set with the cellular

216   genes and pathways previously associated with SARS-CoV-2 replication. To maintain

217   physiological relevance, we restricted our literature search to genes and pathways reported

218   in *ex vivo* SARS-CoV-2-infected primary airway epithelial cells or those identified in blood,

219   bronchioalveolar lavage fluid (BALF) and lung biopsies of SARS-CoV-2 positive patients.

220   Our search identified 55 genes regulated by SNX-5422, which have been associated with

221   SARS-CoV-2 pathogenesis and disease progression. A protein-protein interaction (PPI)

222   network and functional enrichment analysis mapped several of these 55 genes to cellular

223   inflammatory pathways including IL-17 signaling pathway, TNF signaling pathway, cytokine-

224   cytokine receptor interaction and chemokine signaling pathway (Figure 3A). SNX-5422

225   dampened expression of cellular genes, previously shown to be associated with SARS-

226   CoV-2 -mediated proinflammatory response and hyper-cytokinemia (Figure 3B).

227   Specifically, these inflammatory genes could be broadly categorized into chemokines

228   (*CXCL1* (Coperchini et al., 2020)*, CXCL5* (Coperchini et al., 2020)*, CXCL6* (Blanco-Melo et

229   al., 2020)*, CXCL3* (Blanco-Melo et al., 2020) and *CXCL2* (Zhou et al., 2020a)), chemokine-

230   receptor ligands (*CCL20* (Zhou et al., 2020a)*, CX3CL1* (Nienhold et al., 2020)), cytokines

231   (*IL36G* (Xiong et al., 2020)), interleukins (*IL-19* (Vastrad et al., 2020)*, CXCL8* (Zhou et al.,

232   2020a)*, IL-32* (Blanco-Melo et al., 2020)), tumor necrosis factor alpha-induced protein

233   (*TNFAIP2* (Fagone et al., 2020)), regulators of inflammatory responses (*CSF3* (Nunnari et

234   al., 2020)*, S100A8* (Zhou et al., 2020a)*, S100A9* (Zhou et al., 2020a)*, SCGB3A1* (Mick et

235 al., 2020), *S100A2* (Xu et al., 2020)) and interferon-induced proteins (*RSAD2 (Zhou et al.,*

236 *2020a), IFI44L (Mick et al., 2020), IFITM1* (Zhou et al., 2020a), *MX2 (Lieberman et al.,*

237 *2020), IFI27 (*Mick et al., 2020), *ISG15 (Zhou et al., 2020a)*). Collectively, our analysis

238 suggests that early treatment with SNX-5422 may mitigate SARS-CoV-2-mediated

239 hyperinflammation, thereby improving clinical outcomes of COVID-19.

240

241 **SNX-5422 regulates expression of host factors imbalanced upon SARS-CoV-2**

242 **infection.**

243

244 Recently, several host factors of SARS-CoV-2 replication have been identified (Gordon et

245 al., 2020, Wang et al., 2021, Daniloski et al., 2021). Additionally, SARS-CoV-2 infection

246 and COVID-19 progression have been associated with imbalanced expression of cellular

247 pathways (Blanco-Melo et al., 2020) and heightened innate immune responses (Zhou et al.,

248 2020a). Here, we aimed to investigate whether SNX-5422 treatment regulated expression

249 of those previously identified SARS-CoV-2 host factors and cellular mechanisms

250 imbalanced upon infection. Our data indicate that of the 55 genes altered by SNX-5422

251 treatment that were previously reported in the context of SARS-CoV-2 replication (Figure

252 3A), 27 genes had an imbalanced cellular expression, in virally infected cells (Figure 3C).

253 Further categorization of these 55 genes revealed that the majority of these genes fall into

254 4 functional categories,- namely, regulators of innate immunity (*SERPINA3* (D'Alessandro

255 et al., 2020)*, BPIFA1* (Liu et al., 2020)*,* and *PGLYRP4* (Chandrashekar et al., 2020)),

256 regulators of cell cycle (*UBE2C* (Bock and Ortea, 2020)*, CENPI* (Venkatakrishnan et al.,

257 2020)*, BIRC5* (Xiong et al., 2020)*, CCNB2* (Xiong et al., 2020)*, BUB1B* (Ahmed et al.,

258 2020)*, BUB1* (Ahmed et al., 2020) and *CENPF* (Gordon et al., 2020)), mucosal structural

259 proteins (*MMP9* (Hazra et al., 2020) *and FCGBP* (Liu et al., 2020)) and regulators of blood

260 coagulation (*SERPINA3* (D'Alessandro et al., 2020)*, SERPINE1 (McCord et al., 2020) and*

261 *SERPINF2* (D'Alessandro et al., 2020)). Furthermore, cellular genes whose expression was

262 impacted by SNX-5422 treatment, encoded for proteins that were previously shown to be

263 associated with SARS-CoV-2 replication phases (*MMP9* (Hazra et al., 2020) and

264 *SERPINE1 (McCord et al., 2020)*) or those interacting with SARS-CoV-2 structural and

265 non-structural proteins (*BUB1B* (Ahmed et al., 2020)*, BUB1* (Ahmed et al., 2020), *CENPF*

266 (Gordon et al., 2020) and *ID1* (Islam and Khan, 2020)). Taken together, our analysis

267 indicate that SNX-5422 treatment interrupted cellular pathways and genes associated with

268 replication of SARS-CoV-2.

269

270 Viruses rely on the biosynthetic machinery of the host for their replication. Therefore, an

271 attractive strategy to attenuate viral propagation and mitigate poor disease outcomes is to

272 target viral host-dependency factors. While the advantage of such an antiviral strategy is

273 their efficacy against newly evolving viral variants and a high barrier towards development

274 of drug resistant viral strains, such therapies might interfere with the normal cellular

275 functioning. Hence, development of host-targeted therapeutics with very high selectivity index

276 for suppressing viral replication yet having minimal off-target effect is crucial. Moreover, as post-

277 exposure prophylactics are administered to individuals with no-to-mild symptoms, the safety bar

278 for such a therapeutic modality will be higher than those administered in acutely infected

279 patients. Hence, while host-directed drug candidates are currently fast-tracked into clinical trials

280 as anti-SARS-CoV-2 therapeutics, characterizing the interactions of the drug candidates with

281 host cell mechanisms will be absolutely critical to minimize adverse outcomes.

282

283 SARS-CoV-2 infection results in highly activated T cells (Chen and John Wherry, 2020), Th17

284 skewing (De Biasi et al., 2020), activation of the NF-κB signaling pathway (Huang et al., 2020b),

285 and abnormal elevation of inflammatory cytokines (De Biasi et al., 2020), leading to

286 hypercytokinemia and an imbalanced host immune response (Zhou et al., 2020a, Blanco-Melo

11

287 et al., 2020). Hyperinflammation is a key determinant of the severity of COVID-19 outcomes

288 (Mehta et al., 2020), where patients with higher levels of inflammatory cytokines have been

289 associated with higher risk of lung injury and ARDS (Chen et al., 2020, Torres Acosta and

290 Singer, 2020). Hence, targeted treatments, early during the course of infection, to prevent such

291 cytokine storms have been proposed (Gallelli et al., 2020). We demonstrate that SNX-5422-

292 treatment of human TBE cells downregulated key inflammatory pathways and genes associated

293 with poor COVID-19 outcomes (Zhou et al., 2020a, Nienhold et al., 2020). Importantly, SNX-

294 5422 treatment also altered expression of host responses reported to be imbalanced upon

295 SARS-CoV-2 infection such as innate immune responses (Blanco-Melo et al., 2020), cell cycle

296 regulation (Yuan et al., 2006), biosynthesis and metabolism of amino acids (Blasco et al., 2020).

297 Moreover, SNX-5422 interrupted expression of cellular factors that directly or indirectly interact

298 with the crucial steps of SARS-CoV-2 replication (McCord et al., 2020, Hazra et al., 2020) and

299 with viral structural and non-structural proteins (Ahmed et al., 2020, Gordon et al., 2020, Islam

300 and Khan, 2020).

301

302 In summary, our data support further testing and development of SNX-5422 as an oral

303 post-exposure prophylactic or early-phase therapeutic for SARS-CoV-2 infection. Early

304 administration of SNX-5422 will interfere with SARS-CoV-2 replication machinery and dampen

305 virus-induced inflammation and severe disease outcomes, although human trials and

306 experimental validation of such a mechanism in *ex vivo* human primary tissue sections or in

307 animal models remains necessary. Additionally, the fact that SNX-5422 is orally bioavailable,

308 and is clinically tested, makes this drug a quality candidate for an easy-to-administer and

309 rapidly translatable post-exposure prophylactic therapy for SARS-CoV-2 infections. Finally,

310 since SNX-5422 targets dependency factors that are utilized by multiple CoVs (Aldeyra

311 Therapeutics Press Release, 2020, Emanuel et al., 2020, Iyad et al., 2020, Li et al., 2020,

312 Li et al., 2004) this drug may have the potential to serve as a broad-spectrum ready-to-

313   deploy therapeutic, which will be efficacious in not only ending the current pandemic, but also

314   facilitating future pandemic preparedness against newly emerging, genetically diverse, CoV

315   strains.

316

330

331   **AUTHOR CONTRIBUTIONS.** R.G., S.M.P., T.H., M.B. and S.R.P. designed the study and

332   interpreted the data; R.G., J.J.T., F.K., S.N.L., J.S. and M.B. performed experiments and

333   analyzed the data; V.R. performed the RNA-seq and pathway analysis; P.H. and T.H. provided

334   SNX-5422 and consulted on the drug properties. S.M.P., T.H. and M.B. contributed important

335   insights for the interpretation and discussion of the results. R.G. and S.R.P. drafted the

336   manuscript. All authors read and approved the final manuscript.

337

338   **DECLARATIONS OF INTERESTS.** The authors declare no competing interests. A patent has

339   been filed with Duke University for use of SNX-5422 as an anti-SARS-CoV-2 therapeutic.

340

341   **FIGURE TITLES AND LEGENDS.**

342

343   **Figure 1. SNX-5422 potently suppresses SARS-CoV-2 replication at non-toxic**

344   **concentrations.** Vero E6 and Calu-3 cells were infected with SARS-CoV-2 strain USA-

345   WA1/2020 and treated with either 0.1% DMSO (drug-vehicle) or 0.31-2.5µM SNX-5422, or 5µM

346   remdesivir (RDV). Both SNX-5422 and RDV were reconstituted in DMSO. After 48 hr post-

347   infection (pi), (A) Vero cells were immunostained for SARS-CoV-2 nucleocapsid protein (NP)

348   (green). Nuclei was counterstained (blue) prior to imaging. (B) Immunofluorescent images were

349   quantified to evaluate proportions of SARS-CoV-2-NP+ cells. Each symbol and color represent

350   an independent experiment and each data point represents an independent quantified image

351   field. Medians of data points are reported as grey bars. Dotted line represents detection cut off,

352   which is the mean+3 standard deviation (SD) of the percentage of NP+ cells in uninfected

353   controls. Cell-free viral RNA in the supernatant of infected and treated (C) Vero-E6 and (D)

354   Calu-3 cells were measured by qRT-PCR of the viral N gene. The infectious viral titers of the

355   supernatant of (E) Vero E6 and (F) Calu-3 were determined by plaque assay. (G) Vero E6 and

356   (H) Calu-3 cells were treated with either 0.1% DMSO (drug-vehicle) or 0.01-100µM SNX-5422,

357   or 5µM RDV. After 48 hours, proportion of viable cells was evaluated by flow cytometry. Each

358   symbol and color represent an independent experiment and medians of the data points are

359   reported as grey bars.

360

361   **Figure 2. SNX-5422 treatment alters gene expression of human tracheobronchial**

362   **epithelial (TBE) cells.** (A) Schematic diagram illustrating treatment of human TBE cells. TBE

363   cells from 3 independent healthy donors were cultured in air-liquid interface and treated with

14

364   either 0.1% DMSO (drug-vehicle) or 1µM SNX-5422 reconstituted in DMSO, for 48hrs. RNA

365   was then extracted from the cells and bulk RNA sequencing was performed. (B) Volcano plot

366   demonstrating protein coding genes altered upon SNX-5422 treatment of human TBE cells.

367   Red, blue and grey indicates downregulated, upregulated and non-differentially expressed

368   genes, respectively. Differentially expressed genes (DEGs) were defined as protein coding

369   genes with a Log_2 fold change >2 between the drug-treated and control groups and adjusted p

370   value <0.001. Open symbols represent genes with Log_2 fold change >6 between the drug-

371   treated and control groups. Cellular pathway overrepresentation analysis was performed with

372   DEGs with a normalized average read count across donors and experimental conditions ≥300.

373   (C) Downregulated and (D) Upregulated Kyoto Encyclopedia of Genes and Genomes (KEGG)

374   pathways with an adjusted p value< 0.05 were reported. Dot size represented gene ratio and

375   color schema represents adjusted p values.

376

377   **Figure 3. SNX-5422 treatment targets cellular pathways and genes involved in SARS-**

378   **CoV-2 replication and disease progression.** (A) Protein-protein interaction (PPI) network and

379   functional enrichment of genes altered by SNX-5422 that are involved in SARS-CoV-2

380   replication and COVID-19 progression. Each node represents a protein and interactions with

381   confidence score >0.9 are presented. Heat maps of DEGs following SNX-5422 treatment of

382   human TBE cells, that have been identified to be (B) associated with SARS-CoV-2-mediated

383   hyperinflammation and (C) imbalanced upon viral infection. Red represents relative upregulation

384   of gene expression and blue represents relative downregulation of gene expression. Gene

385   expression counts were transformed, and Z score normalized for heat map generation. Donors

386   were clustered with complete linkage. Genes are arranged based on fold changes, as indicated

387   by the fold change key.

388

389

15

390   **TABLE TITLES AND LEGENDS.**

391   **Table 1**. Cell-specific SNX-5422 potency and selectivity

392

393   **METHODS.**

394

395   **Cell cultures.** Fully differentiated human TBE cells (EpiAirway™) from 3 independent donors

396   with no reported respiratory disease or smoking history (Table S1) were obtained from MatTek

397   (Ashland, MA). The cells were cultured at the air-liquid interface in 1 ml of AIR-100-MM culture

398   medium (MatTek) in 6 well plates at 37°C in 5% CO_2. Upon receipt of cells, the cultures were

399   acclimated for 16-24hr prior to the start of experiments. Vero E6 cells (ATCC) were cultured in

400   Dulbecco's modified Eagle's medium (DMEM) supplemented with 10% fetal bovine serum

401   (FBS), 1X Penicillin/Streptomycin (Gibco), and 1X non-essential amino acid (NEAA) mixture

402   (Gibco) and maintained at 37°C in 5% CO_2. Calu-3 cells (ATCC) were cultured in Dulbecco's

403   modified Eagle's medium (DMEM) supplemented with 20% fetal bovine serum (FBS), 25mM

404   HEPES, 1X Penicillin/Streptomycin (Gibco), and maintained at 37°C in 5% CO_2.

405

406   **Compounds.** The small molecular inhibitor of Hsp90, SNX-5422, has been previously

407   described (Fadden et al., 2010, Huang et al., 2009). The compound was synthesized in-house

408   using previously described methods (Duan et al., 2012) and was characterized by proton

409   nuclear magnetic resonance (NMR) and liquid chromatography/mass-spectrometry (LC/MS).

410   The compound was solubilized in 100% DMSO to a 10mM stock concentration. Remdesivir

411   (MedChemExpress LLC, USA) was reconstituted in 100% DMSO to a concentration of 10mM.

412

413   **SARS-CoV-2 propagation and titering.** SARS-CoV-2 USA-WA1/2020 (BEI Resources; NR-

414   52281) was propagated on Vero E6 cells at a multiplicity of infection (MOI) of 0.001 in virus

415   diluent (DMEM supplemented with 2% FBS, 1X Penicillin/Streptomycin (Gibco), 1mM sodium

16

416   pyruvate (Gibco) and 1X NEAA (Gibco)) at 37°C in 5% CO2. At day 4 post-infection (pi), cell

417   supernatant containing the released virus was harvested, spun at 1500 rpm for 5 minutes,

418   filtered through a 0.22μM sterile vacuum filtration system, aliquoted and stored at -80°C until

419   further use.

420

421   Stock viral titer was determined by plaque assay. Briefly, 0.72 X 10^6 Vero E6 cells were seeded

422   in 6 well plates. The stock virus was serially diluted and incubated on cellular monolayer at 37°C

423   in 5% CO2. After 1hr, virus was aspirated, and cells were overlayed with carboxy-methyl

424   cellulose (CMC) containing media (0.6% CMC, MEM supplemented with 1X

425   Penicillin/Streptomycin (Gibco), 2% FBS, 1mM sodium pyruvate (Gibco), 1X NEAA (Gibco),

426   0.3% sodium bicarbonate (Gibco), and 1X GlutaMAX (Gibco). After 4 days of incubation at 37°C

427   in 5% CO2, plaque assays stained with 1% crystal violet in 10% neutral buffered formalin (NBF),

428   and plaque forming unit/mL (Pfu/mL) was determined.

429

430   **SARS-CoV-2 infection and treatment.** 1.4 X 10^5 Vero E6 or Calu-3 cells were seeded in 24

431   well plates. After 24 hrs, cells were incubated with the SARS-CoV-2 isolate at an MOI of 0.01-

432   0.02 at 37°C and 5% CO_2, with intermittent plate rocking. After 1hr, the virus was aspirated,

433   cells were rinsed twice with 1X PBS and fresh maintenance medium containing dilutions of

434   SNX-5422 or Remdesivir or 0.1% DMSO was added. The cells were incubated for 48hrs at

435   37°C and 5% CO_2.

436

437   **Estimation of cellular cytotoxicity using flow cytometry.** Suspensions of Vero E6 and Calu-

438   3 cells were stained with LIVE/DEAD Fixable Aqua Dead Cell Stain kit (Thermo Fisher)

439   according to manufacturer's instructions. The stained cells were fixed using methanol-free 4%

440   formaldehyde (Thermo Fisher) for 30 minutes and acquired on an LSRII flow cytometer (BD

441   Biosciences) using BD FACS Diva software and analyzed with FlowJo software version 10.1

17

442   (Tree Star, Inc). LIVE/DEAD marker negative viable cells were selected from total cells after

443   sequential selection of forward scatter and side scatter singlets.

444

445   **Infectious viral titer of supernatant.** Cellular supernatant was collected from infected and

446   drug-treated cells, 48hrs after infection. The supernatant was clarified by spinning at 1500rpm

447   for 5 minutes and infectious viral titer was measured by plaque assay as described above.

448

449   **qRT-PCR for detecting cell-free viral RNA**.

450   SARS-CoV-2 RNA from cell supernatant was extracted using the QIAamp viral RNA mini kit

451   (Qiagen). A two-step qRT-PCR was used to detect viral RNA released in the cell supernatant. In

452   the first step, viral cDNA for the nucleocapsid (N) gene was generated using SuperScript III

453   Reverse Transcriptase (Invitrogen) and N-reverse primer (5'-GAGGAACGAGAAGAGGCTTG-

454   3'), following manufacturer's instructions. In the second step, 7uL cDNA from step-1 was

455   amplified using N gene forward primer (5'-CACATTGGCACCCGCAATC-3'), N gene reverse

456   primer (5'-GAGGAACGAGAAGAGGCTTG-3') and probe (5'-FAM-

457   ACTTCCTCAAGGAACAACATTGCCA-QSY-3') using Taqman mastermix (Thermo Fisher). The

458   thermal cycling steps were: 50°C for 2 min, 95 °C for 10 min, and 40 cycles of 95 °C for 15 s and

459   60 °C for 1 min, and qPCR was performed on a Step-One-Plus real time PCR machine (Applied

460   Biosystems) using the StepOne Software v2.3. Viral RNA copy number/mL supernatant was

461   assessed using pCDNA3.1(+)-N-eGFP plasmid (GenScript) as standard.

462

463   **Immunofluorescence assay for detection of SARS-CoV-2 N protein.** 1.4×10^5 Vero E6 cells

464   were seeded in 4-well chamber slides (Corning). After 24 hrs, cells were incubated with SARS-

465   CoV-2 USA-WA1/2020 strain at an MOI of 0.01 at 37°C and 5% CO_2, with intermittent rocking.

466   After 1hr, the virus was aspirated, cells were rinsed twice with 1X PBS and fresh maintenance

467   medium containing dilutions of SNX-5422 or Remdesivir or 0.1% DMSO was added. After

468   48hrs, cells were fixed by submerging the chamber slides in 10% NBF for 2hrs. Fixed cells were

469   washed three times with DPBS (Sigma) + 0.02% Triton X-100. For immunostaining, cells were

470   permeabilized with DPBS+ 0.1% Triton-X-100 for 20 minutes and blocked in DPBS

471   supplemented with 5% BSA, 0.02% Tween-20 and 10% donkey sera (Sigma) for 1hr. The cells

472   were then incubated with anti-SARS-CoV-2 N protein antibody (Sinobiological; 1:100) for 2hrs at

473   room temperature. After subsequent washing of the samples, the cells were treated with Alexa

474   Fluor 488 donkey anti-rabbit secondary antibody (Invitrogen; 1:1000) for 1hr at room

475   temperature. After further washing, the coverglasses were mounted on glass slides with

476   ProLong Glass Antifade with NucBlue (Invitrogen) and sealed. Coverglasses were allowed to

477   cure overnight prior to imaging using Axio Imager fluorescent microscope (Carl Zeiss). Images

478   were captured with 20X objective, processed using Zeiss Zen Black software and proportion of

479   SARS-CoV-2-infected cells were counted using Fiji, utilizing the analyze particle function.

480

481   **CC50 and IC50 calculations.** CC50 and IC50 were calculated using Graph Pad Prism using

482   curve fitting.

483

484   **Drug treatment and bulk RNA-sequencing of human TBE cells.** Human TBE cells from 3

485   independent donors (Table S1) were treated with 1μM SNX-5422 or 0.1% DMSO added to the

486   media on the basolateral side of the culture (Figure 2A), in three biological replicates. After

487   48hrs, cells were resuspended in TRIzol reagent (Thermo Fisher) and total RNA from the cells

488   was extracted by phase separation with chloroform and subsequently using the RNeasy Mini Kit

489   (Qiagen). RNA-Seq libraries were prepared using TruSeq RNA library Prep Kit v2 (Illumina, Inc.

490   USA). Before pooling and sequencing, fragment length distribution and library quality were

491   assessed on a TapeStation 2200 (Agilent Technologies), and the libraries were validated by

492   Qubit Fluorometers (Thermo Fisher). All libraries were then pooled in a concentration at 4nM

493   and sequenced on a NextSeq 500 Illumina sequencing platform system using NextSeq 500/550

494   High Output Kit v2.0 (150 cycles) (Illumina, Inc. USA).

495

496   **Analysis of the bulk RNA-seq data.** RNA-Seq data was quality checked with FastQC

497   (Andrews, 2010) and preprocessing was carried out using TrimGalore (Krueger) toolkit to trim

498   low-quality bases and Illumina adapter sequences using default settings. Reads were aligned to

499   the ENSEMBL Homo_sapiens.GRCh38.dna.primary_assembly genome using the ENSEMBL

500   Homo_sapiens.GRCh38.100 transcript (Kersey et al., 2012) annotation file with STAR (Dobin et

501   al., 2013) splice-aware RNA-seq alignment tool in paired mode allowing maximum multimapping

502   of 3. Gene level counts were quantified using FeatureCounts (Liao et al., 2014) tool, counting

503   unique features in non-stranded mode and retaining both gene ID, gene name, and gene

504   biotype mapping from the ENSEMBL annotation file. Prior to differential expression analysis,

505   count data was collapsed to donor level and genes for which mean raw count was at least 15

506   were kept. Normalization and differential expression were carried out with DESeq2 (Love et al.,

507   2014) Bioconductor (Huber et al., 2015) package, utilizing the 'apeglm' Bioconductor package

508   (Zhu et al., 2019) for log fold change shrinkage, in R statistical programming environment. The

509   design formula was constructed to test for the effect of treatment while controlling for donor.

510

511   Principal component analysis (PCA) was performed with plotPCA in 'DESeq2' R package. PCA

512   was done on variance stabilizing transformed (vst) count data and batch corrected with 'limma'

513   package for genes with an average raw count of at least 15 across samples. Volcano plot with

514   differentially expressed genes was generated using 'EnhancedVolcano' package in R, after

515   filtering for described differential expression cutoffs. Heatmaps for differential expression of

516   genes were generated using 'pheatmap' package in R. A vst was applied to count data, and

517   batch corrected with 'limma' package, followed by Z-score normalization. Dot plots

518   demonstrating upregulated and downregulated KEGG pathways were generated using

519   'ClusterProfiler' package in R using a "universe" of all human genes. Protein-protein interaction

520   (PPI) network was constructed using STRING and Cytoscape (vs 3.8.2).

521

522   **Biocontainment and biosafety.** Work with live SARS-CoV-2 isolate (USA-WA1/2020; BEI

523   Resources NR-52281) was performed under Biosafety Level-3 (BSL-3) in the Duke Regional

524   Biocontainment Laboratory.

525

526   **Material availability.** This study did not generate new unique reagents. SNX-5422 can be

527   obtained from T.H upon request.

528

529   **Data and code availability.** The raw and processed RNA-seq data discussed in this publication

530   have been deposited in NCBI's Gene Expression Omnibus and are accessible through GEO

531   Series accession number GSE166397 (https://www.ncbi.nlm.nih.gov/geo/query/acc.cgi?acc=

532   GSE166397).

533

534   **SUPPLEMENTAL INFORMATION.**

535

536   **Figure S1. Sequencing read counts altered upon SNX-5422 treatment of human TBE**

537   **cells.** Principal component analysis (PCA) of gene expression counts in human TBE cells

538   treated with 0.1% DMSO (circles) or 1μM SNX-5422. (triangles). Each donor is indicated by a

539   single color and 3 biological replicates from each donor are plotted. Red and blue oval symbols

540   represent SNX-5422 and DMSO-treated clusters, respectively.

541

542   **Table S1.** Human Tracheobronchial cell (TBE) donor information.

543

544 **Table S2.** Differentially expressed genes (DEGs) used for cellular pathway overrepresentation

545 analysis.

546

547 **REFERENCES**.

548

549 AHMED, S., PARAMASIVAM, P., RAJ, K., KUMAR, V., MURUGESAN, R. & RAMAKRISHNAN,
550   V. 2020. Regulatory Cross Talk Between SARS-CoV-2 Receptor Binding and
551   Replication Machinery in the Human Host. *Front Physiol,* 11**,** 802.
552 ALDEYRA THERAPEUTICS PRESS RELEASE. 2020. *Aldeyra Therapeutics to Advance ADX-*
553   *1612, an Investigational New HSP90 Inhibitor with Potential Nanomolar Potency Against*
554   *SARS-CoV-2, to Clinical Testing for COVID-19; ADX-629 Accepted for BARDA*
555   *CoronaWatch Meeting* [Online]. Available: https://ir.aldeyra.com/news-releases/news-
556   release-details/aldeyra-therapeutics-advance-adx-1612-investigational-new-hsp90
557   [Accessed].
558 ANDREWS, S. 2010. *FastQC: a quality control tool for high throughput sequence data.* [Online].
559   Available: http://www.bioinformatics.babraham.ac.uk/projects/fastqc/ [Accessed].
560 BEIGEL, J. H., TOMASHEK, K. M., DODD, L. E., MEHTA, A. K., ZINGMAN, B. S., KALIL, A. C.,
561   HOHMANN, E., CHU, H. Y., LUETKEMEYER, A., KLINE, S., LOPEZ DE CASTILLA, D.,
562   FINBERG, R. W., DIERBERG, K., TAPSON, V., HSIEH, L., PATTERSON, T. F.,
563   PAREDES, R., SWEENEY, D. A., SHORT, W. R., TOULOUMI, G., LYE, D. C.,
564   OHMAGARI, N., OH, M. D., RUIZ-PALACIOS, G. M., BENFIELD, T., FATKENHEUER,
565   G., KORTEPETER, M. G., ATMAR, R. L., CREECH, C. B., LUNDGREN, J., BABIKER,
566   A. G., PETT, S., NEATON, J. D., BURGESS, T. H., BONNETT, T., GREEN, M.,
567   MAKOWSKI, M., OSINUSI, A., NAYAK, S., LANE, H. C. & MEMBERS, A.-S. G. 2020.
568   Remdesivir for the Treatment of Covid-19 - Final Report. *N Engl J Med,* 383**,** 1813-1826.
569 BLANCO-MELO, D., NILSSON-PAYANT, B. E., LIU, W. C., UHL, S., HOAGLAND, D.,
570   MOLLER, R., JORDAN, T. X., OISHI, K., PANIS, M., SACHS, D., WANG, T. T.,
571   SCHWARTZ, R. E., LIM, J. K., ALBRECHT, R. A. & TENOEVER, B. R. 2020.
572   Imbalanced Host Response to SARS-CoV-2 Drives Development of COVID-19. *Cell,*
573   181**,** 1036-1045 e9.
574 BLASCO, H., BESSY, C., PLANTIER, L., LEFEVRE, A., PIVER, E., BERNARD, L., MARLET,
575   J., STEFIC, K., BENZ-DE BRETAGNE, I., CANNET, P., LUMBU, H., MOREL, T.,
576   BOULARD, P., ANDRES, C. R., VOURC'H, P., HÉRAULT, O., GUILLON, A. & EMOND,
577   P. 2020. The specific metabolome profiling of patients infected by SARS-COV-2
578   supports the key role of tryptophan-nicotinamide pathway and cytosine metabolism.
579   *Scientific Reports,* 10**,** 16824.
580 BOCK, J. O. & ORTEA, I. 2020. Re-analysis of SARS-CoV-2-infected host cell proteomics time-
581   course data by impact pathway analysis and network analysis: a potential link with
582   inflammatory response. *Aging (Albany NY),* 12**,** 11277-11286.
583 BUSSANI, R., SCHNEIDER, E., ZENTILIN, L., COLLESI, C., ALI, H., BRAGA, L., VOLPE, M.
584   C., COLLIVA, A., ZANCONATI, F., BERLOT, G., SILVESTRI, F., ZACCHIGNA, S. &
585   GIACCA, M. 2020. Persistence of viral RNA, pneumocyte syncytia and thrombosis are
586   hallmarks of advanced COVID-19 pathology. *EBioMedicine,* 61**,** 103104.
587 CHANDRASHEKAR, D. S., MANNE, U. & VARAMBALLY, S. 2020. Comparative transcriptome
588   analyses reveal genes associated with SARS-CoV-2 infection of human lung epithelial
589   cells. *bioRxiv,* 2020.06.24.169268.

590 CHATTERJEE, A., DIMITROPOULOU, C., DRAKOPANAYIOTAKIS, F., ANTONOVA, G.,
591   SNEAD, C., CANNON, J., VENEMA, R. C. & CATRAVAS, J. D. 2007. Heat shock
592   protein 90 inhibitors prolong survival, attenuate inflammation, and reduce lung injury in
593   murine sepsis. *Am J Respir Crit Care Med,* 176**,** 667-75.
594 CHEN, L.-D., ZHANG, Z.-Y., WEI, X.-J., CAI, Y.-Q., YAO, W.-Z., WANG, M.-H., HUANG, Q.-F.
595   & ZHANG, X.-B. 2020. Association between cytokine profiles and lung injury in COVID-
596   19 pneumonia. *Respiratory Research,* 21**,** 201.
597 CHEN, Z. & JOHN WHERRY, E. 2020. T cell responses in patients with COVID-19. *Nat Rev*
598   *Immunol,* 20**,** 529-536.
599 COPERCHINI, F., CHIOVATO, L., CROCE, L., MAGRI, F. & ROTONDI, M. 2020. The cytokine
600   storm in COVID-19: An overview of the involvement of the chemokine/chemokine-
601   receptor system. *Cytokine Growth Factor Rev,* 53**,** 25-32.
602 CUCINOTTA, D. & VANELLI, M. 2020. WHO Declares COVID-19 a Pandemic. *Acta Biomed,*
603   91**,** 157-160.
604 D'ALESSANDRO, A., THOMAS, T., DZIECIATKOWSKA, M., HILL, R. C., FRANCIS, R. O.,
605   HUDSON, K. E., ZIMRING, J. C., HOD, E. A., SPITALNIK, S. L. & HANSEN, K. C. 2020.
606   Serum Proteomics in COVID-19 Patients: Altered Coagulation and Complement Status
607   as a Function of IL-6 Level. *J Proteome Res,* 19**,** 4417-4427.
608 DANILOSKI, Z., JORDAN, T. X., WESSELS, H. H., HOAGLAND, D. A., KASELA, S., LEGUT,
609   M., MANIATIS, S., MIMITOU, E. P., LU, L., GELLER, E., DANZIGER, O.,
610   ROSENBERG, B. R., PHATNANI, H., SMIBERT, P., LAPPALAINEN, T., TENOEVER, B.
611   R. & SANJANA, N. E. 2021. Identification of Required Host Factors for SARS-CoV-2
612   Infection in Human Cells. *Cell,* 184**,** 92-105 e16.
613 DE BIASI, S., MESCHIARI, M., GIBELLINI, L., BELLINAZZI, C., BORELLA, R., FIDANZA, L.,
614   GOZZI, L., IANNONE, A., LO TARTARO, D., MATTIOLI, M., PAOLINI, A., MENOZZI,
615   M., MILIĆ, J., FRANCESCHI, G., FANTINI, R., TONELLI, R., SITA, M., SARTI, M.,
616   TRENTI, T., BRUGIONI, L., CICCHETTI, L., FACCHINETTI, F., PIETRANGELO, A.,
617   CLINI, E., GIRARDIS, M., GUARALDI, G., MUSSINI, C. & COSSARIZZA, A. 2020.
618   Marked T cell activation, senescence, exhaustion and skewing towards TH17 in patients
619   with COVID-19 pneumonia. *Nature Communications,* 11**,** 3434.
620 DOBIN, A., DAVIS, C. A., SCHLESINGER, F., DRENKOW, J., ZALESKI, C., JHA, S., BATUT,
621   P., CHAISSON, M. & GINGERAS, T. R. 2013. STAR: ultrafast universal RNA-seq
622   aligner. *Bioinformatics,* 29**,** 15-21.
623 DUAN, S., VENKATRAMAN, S., HONG, X., HUANG, K., ULYSSE, L., MOBELE, B. I., SMITH,
624   A., LAWLESS, L., LOCKE, A. & GARIGIPATI, R. 2012. Process Development and
625   Scale-Up of an Hsp90 Inhibitor. *Organic Process Research & Development,* 16**,** 1787-
626   1793.
627 EMANUEL, W., KIRSTIN, M., VEDRAN, F., ASIJA, D., THERESA, G. L., ROBERTO, A.,
628   FILIPPOS, K., DAVID, K., SALAH, A., CHRISTOPHER, B., ANJA, R., IVANO, L.,
629   ANDRANIK, I., TOMMASO, M., SIMONE, D. G., PATRICK, P. J., ALEXANDER, M. M.,
630   DANIELA, N., MATTHIAS, S., ALTUNA, A., NIKOLAUS, R., CHRISTIAN, D. &
631   MARKUS, L. 2020. Bulk and single-cell gene expression profiling of SARS-CoV-2
632   infected human cell lines identifies molecular targets for therapeutic intervention.
633   *bioRxiv***,** 2020.05.05.079194.
634 FADDEN, P., HUANG, K. H., VEAL, J. M., STEED, P. M., BARABASZ, A. F., FOLEY, B., HU,
635   M., PARTRIDGE, J. M., RICE, J., SCOTT, A., DUBOIS, L. G., FREED, T. A., SILINSKI,
636   M. A., BARTA, T. E., HUGHES, P. F., OMMEN, A., MA, W., SMITH, E. D.,
637   SPANGENBERG, A. W., EAVES, J., HANSON, G. J., HINKLEY, L., JENKS, M., LEWIS,
638   M., OTTO, J., PRONK, G. J., VERLEYSEN, K., HAYSTEAD, T. A. & HALL, S. E. 2010.
639   Application of chemoproteomics to drug discovery: identification of a clinical candidate
640   targeting hsp90. *Chem Biol,* 17**,** 686-94.

FAGONE, P., CIURLEO, R., LOMBARDO, S. D., IACOBELLO, C., PALERMO, C. I., SHOENFELD, Y., BENDTZEN, K., BRAMANTI, P. & NICOLETTI, F. 2020. Transcriptional landscape of SARS-CoV-2 infection dismantles pathogenic pathways activated by the virus, proposes unique sex-specific differences and predicts tailored therapeutic strategies. *Autoimmun Rev,* 19**,** 102571.

GALLELLI, L., ZHANG, L., WANG, T. & FU, F. 2020. Severe Acute Lung Injury Related to COVID-19 Infection: A Review and the Possible Role for Escin. *J Clin Pharmacol,* 60**,** 815-825.

GELLER, R., TAGUWA, S. & FRYDMAN, J. 2012. Broad action of Hsp90 as a host chaperone required for viral replication. *Biochim Biophys Acta,* 1823**,** 698-706.

GELLER, R., VIGNUZZI, M., ANDINO, R. & FRYDMAN, J. 2007. Evolutionary constraints on chaperone-mediated folding provide an antiviral approach refractory to development of drug resistance. *Genes Dev,* 21**,** 195-205.

GIAMARELLOS-BOURBOULIS, E. J., NETEA, M. G., ROVINA, N., AKINOSOGLOU, K., ANTONIADOU, A., ANTONAKOS, N., DAMORAKI, G., GKAVOGIANNI, T., ADAMI, M. E., KATSAOUNOU, P., NTAGANOU, M., KYRIAKOPOULOU, M., DIMOPOULOS, G., KOUTSODIMITROPOULOS, I., VELISSARIS, D., KOUFARGYRIS, P., KARAGEORGOS, A., KATRINI, K., LEKAKIS, V., LUPSE, M., KOTSAKI, A., RENIERIS, G., THEODOULOU, D., PANOU, V., KOUKAKI, E., KOULOURIS, N., GOGOS, C. & KOUTSOUKOU, A. 2020. Complex Immune Dysregulation in COVID-19 Patients with Severe Respiratory Failure. *Cell Host Microbe,* 27**,** 992-1000 e3.

GORDON, D. E., JANG, G. M., BOUHADDOU, M., XU, J., OBERNIER, K., WHITE, K. M., O'MEARA, M. J., REZELJ, V. V., GUO, J. Z., SWANEY, D. L., TUMMINO, T. A., HUTTENHAIN, R., KAAKE, R. M., RICHARDS, A. L., TUTUNCUOGLU, B., FOUSSARD, H., BATRA, J., HAAS, K., MODAK, M., KIM, M., HAAS, P., POLACCO, B. J., BRABERG, H., FABIUS, J. M., ECKHARDT, M., SOUCHERAY, M., BENNETT, M. J., CAKIR, M., MCGREGOR, M. J., LI, Q., MEYER, B., ROESCH, F., VALLET, T., MAC KAIN, A., MIORIN, L., MORENO, E., NAING, Z. Z. C., ZHOU, Y., PENG, S., SHI, Y., ZHANG, Z., SHEN, W., KIRBY, I. T., MELNYK, J. E., CHORBA, J. S., LOU, K., DAI, S. A., BARRIO-HERNANDEZ, I., MEMON, D., HERNANDEZ-ARMENTA, C., LYU, J., MATHY, C. J. P., PERICA, T., PILLA, K. B., GANESAN, S. J., SALTZBERG, D. J., RAKESH, R., LIU, X., ROSENTHAL, S. B., CALVIELLO, L., VENKATARAMANAN, S., LIBOY-LUGO, J., LIN, Y., HUANG, X. P., LIU, Y., WANKOWICZ, S. A., BOHN, M., SAFARI, M., UGUR, F. S., KOH, C., SAVAR, N. S., TRAN, Q. D., SHENGJULER, D., FLETCHER, S. J., O'NEAL, M. C., CAI, Y., CHANG, J. C. J., BROADHURST, D. J., KLIPPSTEN, S., SHARP, P. P., WENZELL, N. A., KUZUOGLU-OZTURK, D., WANG, H. Y., TRENKER, R., YOUNG, J. M., CAVERO, D. A., HIATT, J., ROTH, T. L., RATHORE, U., SUBRAMANIAN, A., NOACK, J., HUBERT, M., STROUD, R. M., FRANKEL, A. D., ROSENBERG, O. S., VERBA, K. A., AGARD, D. A., OTT, M., EMERMAN, M., JURA, N., et al. 2020. A SARS-CoV-2 protein interaction map reveals targets for drug repurposing. *Nature,* 583**,** 459-468.

HAZRA, S., CHAUDHURI, A. G., TIWARY, B. K. & CHAKRABARTI, N. 2020. Matrix metallopeptidase 9 as a host protein target of chloroquine and melatonin for immunoregulation in COVID-19: A network-based meta-analysis. *Life Sci,* 257**,** 118096.

HUANG, C., WANG, Y., LI, X., REN, L., ZHAO, J., HU, Y., ZHANG, L., FAN, G., XU, J., GU, X., CHENG, Z., YU, T., XIA, J., WEI, Y., WU, W., XIE, X., YIN, W., LI, H., LIU, M., XIAO, Y., GAO, H., GUO, L., XIE, J., WANG, G., JIANG, R., GAO, Z., JIN, Q., WANG, J. & CAO, B. 2020a. Clinical features of patients infected with 2019 novel coronavirus in Wuhan, China. *Lancet,* 395**,** 497-506.

HUANG, J., HUME, A. J., ABO, K. M., WERDER, R. B., VILLACORTA-MARTIN, C., ALYSANDRATOS, K. D., BEERMANN, M. L., SIMONE-ROACH, C., LINDSTROM-

VAUTRIN, J., OLEJNIK, J., SUDER, E. L., BULLITT, E., HINDS, A., SHARMA, A., BOSMANN, M., WANG, R., HAWKINS, F., BURKS, E. J., SAEED, M., WILSON, A. A., MUHLBERGER, E. & KOTTON, D. N. 2020b. SARS-CoV-2 Infection of Pluripotent Stem Cell-derived Human Lung Alveolar Type 2 Cells Elicits a Rapid Epithelial-Intrinsic Inflammatory Response. *bioRxiv*.

HUANG, K. H., VEAL, J. M., FADDEN, R. P., RICE, J. W., EAVES, J., STRACHAN, J. P., BARABASZ, A. F., FOLEY, B. E., BARTA, T. E., MA, W., SILINSKI, M. A., HU, M., PARTRIDGE, J. M., SCOTT, A., DUBOIS, L. G., FREED, T., STEED, P. M., OMMEN, A. J., SMITH, E. D., HUGHES, P. F., WOODWARD, A. R., HANSON, G. J., MCCALL, W. S., MARKWORTH, C. J., HINKLEY, L., JENKS, M., GENG, L., LEWIS, M., OTTO, J., PRONK, B., VERLEYSEN, K. & HALL, S. E. 2009. Discovery of novel 2-aminobenzamide inhibitors of heat shock protein 90 as potent, selective and orally active antitumor agents. *J Med Chem,* 52**,** 4288-305.

HUBER, W., CAREY, V. J., GENTLEMAN, R., ANDERS, S., CARLSON, M., CARVALHO, B. S., BRAVO, H. C., DAVIS, S., GATTO, L., GIRKE, T., GOTTARDO, R., HAHNE, F., HANSEN, K. D., IRIZARRY, R. A., LAWRENCE, M., LOVE, M. I., MACDONALD, J., OBENCHAIN, V., OLES, A. K., PAGES, H., REYES, A., SHANNON, P., SMYTH, G. K., TENENBAUM, D., WALDRON, L. & MORGAN, M. 2015. Orchestrating high-throughput genomic analysis with Bioconductor. *Nat Methods,* 12**,** 115-21.

INFANTE, J. R., WEISS, G. J., JONES, S., TIBES, R., BAUER, T. M., BENDELL, J. C., HINSON, J. M., JR., VON HOFF, D. D., BURRIS, H. A., 3RD, ORLEMANS, E. O. & RAMANATHAN, R. K. 2014. Phase I dose-escalation studies of SNX-5422, an orally bioavailable heat shock protein 90 inhibitor, in patients with refractory solid tumours. *Eur J Cancer,* 50**,** 2897-904.

ISLAM, A. & KHAN, M. A. 2020. Lung transcriptome of a COVID-19 patient and systems biology predictions suggest impaired surfactant production which may be druggable by surfactant therapy. *Sci Rep,* 10**,** 19395.

IYAD, S., SCOTT, H. & ABDELGHANI, T. 2020. Drug Repositioning Suggests a Role for the Heat Shock Protein 90 Inhibitor Geldanamycin in Treating COVID-19 Infection. *22 March 2020, PREPRINT (Version 1)*

KAMEL, W., NOERENBERG, M., CERIKAN, B., CHEN, H., JÄRVELIN, A., KAMMOUN, M., LEE, J., SHUAI, N., GARCIA-MORENO, M., ANDREJEVA, A., DEERY, M., NEUFELDT, C., CORTESE, M., KNIGHT, M., LILLEY, K., MARTINEZ, J., DAVIS, I., BARTENSCHLAGER, R., MOHAMMED, S. & CASTELLO, A. 2020. Global analysis of protein-RNA interactions in SARS-CoV-2 infected cells reveals key regulators of infection. bioRxiv.

KERSEY, P. J., STAINES, D. M., LAWSON, D., KULESHA, E., DERWENT, P., HUMPHREY, J. C., HUGHES, D. S., KEENAN, S., KERHORNOU, A., KOSCIELNY, G., LANGRIDGE, N., MCDOWALL, M. D., MEGY, K., MAHESWARI, U., NUHN, M., PAULINI, M., PEDRO, H., TONEVA, I., WILSON, D., YATES, A. & BIRNEY, E. 2012. Ensembl Genomes: an integrative resource for genome-scale data from non-vertebrate species. *Nucleic Acids Res,* 40**,** D91-7.

KRUEGER, F. *A wrapper tool around Cutadapt and FastQC to consistently apply quality and adapter trimming to FastQ files, with some extra functionality for MspI-digested RRBS-type (Reduced Representation Bisufite-Seq) libraries.* [Online]. Available: http://www.bioinformatics.babraham.ac.uk/projects/trim_galore/ [Accessed].

LI, C., CHU, H., LIU, X., CHIU, M. C., ZHAO, X., WANG, D., WEI, Y., HOU, Y., SHUAI, H., CAI, J., CHAN, J. F., ZHOU, J. & YUEN, K. Y. 2020. Human coronavirus dependency on host heat shock protein 90 reveals an antiviral target. *Emerg Microbes Infect,* 9**,** 2663-2672.

25

LI, Y. H., TAO, P. Z., LIU, Y. Z. & JIANG, J. D. 2004. Geldanamycin, a ligand of heat shock protein 90, inhibits the replication of herpes simplex virus type 1 in vitro. *Antimicrob Agents Chemother,* 48**,** 867-72.

LIAO, Y., SMYTH, G. K. & SHI, W. 2014. featureCounts: an efficient general purpose program for assigning sequence reads to genomic features. *Bioinformatics,* 30**,** 923-30.

LIEBERMAN, N. A. P., PEDDU, V., XIE, H., SHRESTHA, L., HUANG, M.-L., MEARS, M. C., CAJIMAT, M. N., BENTE, D. A., SHI, P.-Y., BOVIER, F., ROYCHOUDHURY, P., JEROME, K. R., MOSCONA, A., POROTTO, M. & GRENINGER, A. L. 2020. In vivo antiviral host transcriptional response to SARS-CoV-2 by viral load, sex, and age. *PLOS Biology,* 18**,** e3000849.

LIU, T., JIA, P., FANG, B. & ZHAO, Z. 2020. Differential Expression of Viral Transcripts From Single-Cell RNA Sequencing of Moderate and Severe COVID-19 Patients and Its Implications for Case Severity. *Frontiers in Microbiology,* 11.

LOVE, M. I., HUBER, W. & ANDERS, S. 2014. Moderated estimation of fold change and dispersion for RNA-seq data with DESeq2. *Genome Biol,* 15**,** 550.

MASON, R. J. 2020. Pathogenesis of COVID-19 from a cell biology perspective. *Eur Respir J,* 55.

MCCORD, J. M., HYBERTSON, B. M., COTA-GOMEZ, A. & GAO, B. 2020. Nrf2 Activator PB125(R) as a Potential Therapeutic Agent Against COVID-19. *bioRxiv.*

MEHRAEEN, E., KARIMI, A., BARZEGARY, A., VAHEDI, F., AFSAHI, A. M., DADRAS, O., MORADMAND-BADIE, B., SEYED ALINAGHI, S. A. & JAHANFAR, S. 2020. Predictors of mortality in patients with COVID-19-a systematic review. *Eur J Integr Med,* 40**,** 101226.

MEHTA, P., MCAULEY, D. F., BROWN, M., SANCHEZ, E., TATTERSALL, R. S., MANSON, J. J. & HLH ACROSS SPECIALITY COLLABORATION, U. K. 2020. COVID-19: consider cytokine storm syndromes and immunosuppression. *Lancet,* 395**,** 1033-1034.

MICK, E., KAMM, J., PISCO, A. O., RATNASIRI, K., BABIK, J. M., CALFEE, C. S., CASTANEDA, G., DERISI, J. L., DETWEILER, A. M., HAO, S., KANGELARIS, K. N., KUMAR, G. R., LI, L. M., MANN, S. A., NEFF, N., PRASAD, P. A., SERPA, P. H., SHAH, S. J., SPOTTISWOODE, N., TAN, M., CHRISTENSON, S. A., KISTLER, A. & LANGELIER, C. 2020. Upper airway gene expression differentiates COVID-19 from other acute respiratory illnesses and reveals suppression of innate immune responses by SARS-CoV-2. *medRxiv.*

NIENHOLD, R., CIANI, Y., KOELZER, V. H., TZANKOV, A., HASLBAUER, J. D., MENTER, T., SCHWAB, N., HENKEL, M., FRANK, A., ZSIKLA, V., WILLI, N., KEMPF, W., HOYLER, T., BARBARESCHI, M., MOCH, H., TOLNAY, M., CATHOMAS, G., DEMICHELIS, F., JUNT, T. & MERTZ, K. D. 2020. Two distinct immunopathological profiles in autopsy lungs of COVID-19. *Nature Communications,* 11**,** 5086.

NISHIURA, H., KOBAYASHI, T., MIYAMA, T., SUZUKI, A., JUNG, S. M., HAYASHI, K., KINOSHITA, R., YANG, Y., YUAN, B., AKHMETZHANOV, A. R. & LINTON, N. M. 2020. Estimation of the asymptomatic ratio of novel coronavirus infections (COVID-19). *Int J Infect Dis,* 94**,** 154-155.

NITULESCU, G. M., PAUNESCU, H., MOSCHOS, S. A., PETRAKIS, D., NITULESCU, G., ION, G. N. D., SPANDIDOS, D. A., NIKOLOUZAKIS, T. K., DRAKOULIS, N. & TSATSAKIS, A. 2020. Comprehensive analysis of drugs to treat SARSCoV2 infection: Mechanistic insights into current COVID19 therapies (Review). *Int J Mol Med,* 46**,** 467-488.

NUNNARI, G., SANFILIPPO, C., CASTROGIOVANNI, P., IMBESI, R., LI VOLTI, G., BARBAGALLO, I., MUSUMECI, G. & DI ROSA, M. 2020. Network perturbation analysis in human bronchial epithelial cells following SARS-CoV2 infection. *Exp Cell Res,* 395**,** 112204.

791 OGANDO, N. S., DALEBOUT, T. J., ZEVENHOVEN-DOBBE, J. C., LIMPENS, R., VAN DER
792   MEER, Y., CALY, L., DRUCE, J., DE VRIES, J. J. C., KIKKERT, M., BARCENA, M.,
793   SIDOROV, I. & SNIJDER, E. J. 2020. SARS-coronavirus-2 replication in Vero E6 cells:
794   replication kinetics, rapid adaptation and cytopathology. *J Gen Virol,* 101**,** 925-940.
795 OKAWA, Y., HIDESHIMA, T., STEED, P., VALLET, S., HALL, S., HUANG, K., RICE, J.,
796   BARABASZ, A., FOLEY, B., IKEDA, H., RAJE, N., KIZILTEPE, T., YASUI, H., ENATSU,
797   S. & ANDERSON, K. C. 2009. SNX-2112, a selective Hsp90 inhibitor, potently inhibits
798   tumor cell growth, angiogenesis, and osteoclastogenesis in multiple myeloma and other
799   hematologic tumors by abrogating signaling via Akt and ERK. *Blood,* 113**,** 846-55.
800 PANDOLFI, L., FOSSALI, T., FRANGIPANE, V., BOZZINI, S., MOROSINI, M., D'AMATO, M.,
801   LETTIERI, S., URTIS, M., DI TORO, A., SARACINO, L., PERCIVALLE, E., TOMASELLI,
802   S., CAVAGNA, L., COVA, E., MOJOLI, F., BERGOMI, P., OTTOLINA, D., LILLERI, D.,
803   CORSICO, A. G., ARBUSTINI, E., COLOMBO, R. & MELONI, F. 2020. Broncho-alveolar
804   inflammation in COVID-19 patients: a correlation with clinical outcome. *BMC Pulm Med,*
805   20**,** 301.
806 PRESCOTT, H. C. & RICE, T. W. 2020. Corticosteroids in COVID-19 ARDS: Evidence and
807   Hope During the Pandemic. *JAMA,* 324**,** 1292-1295.
808 RAJAN, A., KELLY, R. J., TREPEL, J. B., KIM, Y. S., ALARCON, S. V., KUMMAR, S.,
809   GUTIERREZ, M., CRANDON, S., ZEIN, W. M., JAIN, L., MANNARGUDI, B., FIGG, W.
810   D., HOUK, B. E., SHNAIDMAN, M., BREGA, N. & GIACCONE, G. 2011. A phase I study
811   of PF-04929113 (SNX-5422), an orally bioavailable heat shock protein 90 inhibitor, in
812   patients with refractory solid tumor malignancies and lymphomas. *Clin Cancer Res,* 17**,**
813   6831-9.
814 RATHORE, A. P., HAYSTEAD, T., DAS, P. K., MERITS, A., NG, M. L. & VASUDEVAN, S. G.
815   2014. Chikungunya virus nsP3 & nsP4 interacts with HSP-90 to promote virus
816   replication: HSP-90 inhibitors reduce CHIKV infection and inflammation in vivo. *Antiviral*
817   *Res,* 103**,** 7-16.
818 SMITH, A. P. & HAYSTEAD, T. A. J. 2017. Hsp90: a key target in HIV infection. *Future Virology,*
819   12**,** 55-59.
820 SONG, P., LI, W., XIE, J., HOU, Y. & YOU, C. 2020. Cytokine storm induced by SARS-CoV-2.
821   *Clin Chim Acta,* 509**,** 280-287.
822 TAIPALE, M., JAROSZ, D. F. & LINDQUIST, S. 2010. HSP90 at the hub of protein
823   homeostasis: emerging mechanistic insights. *Nat Rev Mol Cell Biol,* 11**,** 515-28.
824 TORRES ACOSTA, M. A. & SINGER, B. D. 2020. Pathogenesis of COVID-19-induced ARDS:
825   implications for an ageing population. *Eur Respir J,* 56.
826 VASTRAD, B., VASTRAD, C. & TENGLI, A. 2020. Identification of potential mRNA panels for
827   severe acute respiratory syndrome coronavirus 2 (COVID-19) diagnosis and treatment
828   using microarray dataset and bioinformatics methods. *3 Biotech,* 10**,** 422.
829 VENKATAKRISHNAN, A. J., KAYAL, N., ANAND, P., BADLEY, A. D., CHURCH, G. M. &
830   SOUNDARARAJAN, V. 2020. Benchmarking evolutionary tinkering underlying human–
831   viral molecular mimicry shows multiple host pulmonary–arterial peptides mimicked by
832   SARS-CoV-2. *Cell Death Discovery,* 6**,** 96.
833 WANG, R., SIMONEAU, C. R., KULSUPTRAKUL, J., BOUHADDOU, M., TRAVISANO, K. A.,
834   HAYASHI, J. M., CARLSON-STEVERMER, J., ZENGEL, J. R., RICHARDS, C. M.,
835   FOZOUNI, P., OKI, J., RODRIGUEZ, L., JOEHNK, B., WALCOTT, K., HOLDEN, K., SIL,
836   A., CARETTE, J. E., KROGAN, N. J., OTT, M. & PUSCHNIK, A. S. 2021. Genetic
837   Screens Identify Host Factors for SARS-CoV-2 and Common Cold Coronaviruses. *Cell,*
838   184**,** 106-119 e14.
839 WHO CORONAVIRUS DISEASE (COVID-19) DASHBOARD. 2020.
840   *https://covid19.who.int/?gclid=Cj0KCQiAmL-*
841   *ABhDFARIsAKywVafJxVkqo9vmNjGaiJEw5SEQU7xbiPnPU7_Wwnflc3xMAkp7QwF1C*

842   *HMaAijZEALw_wcB* [Online]. Available: https://covid19.who.int/?gclid=Cj0KCQiAmL-
843   ABhDFARIsAKywVafJxVkqo9vmNjGaiJEw5SEQU7xbiPnPU7_WwnfIc3xMAkp7QwF1C
844   HMaAijZEALw_wcB [Accessed].
845 XIONG, Y., LIU, Y., CAO, L., WANG, D., GUO, M., JIANG, A., GUO, D., HU, W., YANG, J.,
846   TANG, Z., WU, H., LIN, Y., ZHANG, M., ZHANG, Q., SHI, M., LIU, Y., ZHOU, Y., LAN,
847   K. & CHEN, Y. 2020. Transcriptomic characteristics of bronchoalveolar lavage fluid and
848   peripheral blood mononuclear cells in COVID-19 patients. *Emerg Microbes Infect,* 9**,**
849   761-770.
850 XU, G., QI, F., LI, H., YANG, Q., WANG, H., WANG, X., LIU, X., ZHAO, J., LIAO, X., LIU, Y.,
851   LIU, L., ZHANG, S. & ZHANG, Z. 2020. The differential immune responses to COVID-19
852   in peripheral and lung revealed by single-cell RNA sequencing. *Cell Discovery,* 6**,** 73.
853 YUAN, X., WU, J., SHAN, Y., YAO, Z., DONG, B., CHEN, B., ZHAO, Z., WANG, S., CHEN, J. &
854   CONG, Y. 2006. SARS coronavirus 7a protein blocks cell cycle progression at G0/G1
855   phase via the cyclin D3/pRb pathway. *Virology,* 346**,** 74-85.
856 ZHAO, R. & HOURY, W. A. 2005. Hsp90: a chaperone for protein folding and gene regulation.
857   *Biochem Cell Biol,* 83**,** 703-10.
858 ZHOU, Z., REN, L., ZHANG, L., ZHONG, J., XIAO, Y., JIA, Z., GUO, L., YANG, J., WANG, C.,
859   JIANG, S., YANG, D., ZHANG, G., LI, H., CHEN, F., XU, Y., CHEN, M., GAO, Z., YANG,
860   J., DONG, J., LIU, B., ZHANG, X., WANG, W., HE, K., JIN, Q., LI, M. & WANG, J.
861   2020a. Heightened Innate Immune Responses in the Respiratory Tract of COVID-19
862   Patients. *Cell Host Microbe,* 27**,** 883-890 e2.
863 ZHOU, Z., WANG, X., FU, Y., ZHANG, X. & LIU, C. 2020b. Neutralizing antibodies for the
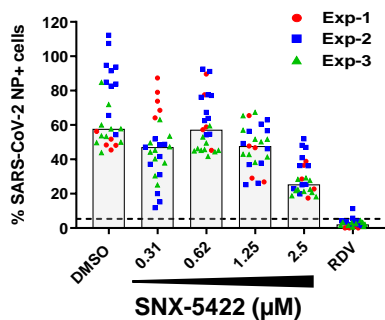864   treatment of COVID-19. *Acta Pharm Sin B.*
865 ZHU, A., IBRAHIM, J. G. & LOVE, M. I. 2019. Heavy-tailed prior distributions for sequence
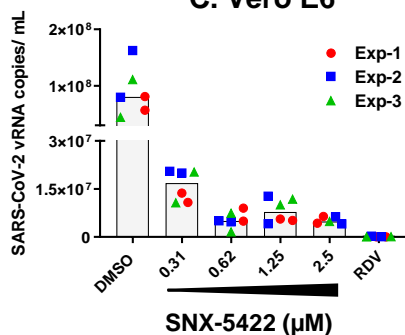866   count data: removing the noise and preserving large differences. *Bioinformatics,* 35**,**
867   2084-2092.

868

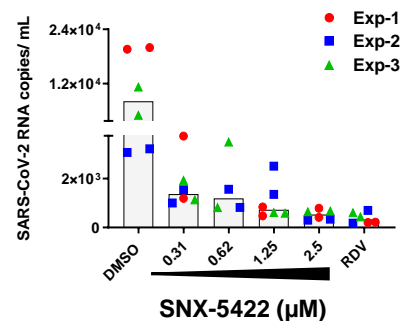**A. SARS-CoV-2 N protein (NP) expression**

Nuclei / NP / Merged

DMSO   0.31   0.62   1.25   2.5   RDV

SNX-5422 (μM)

B. Proportion of NP+ cells
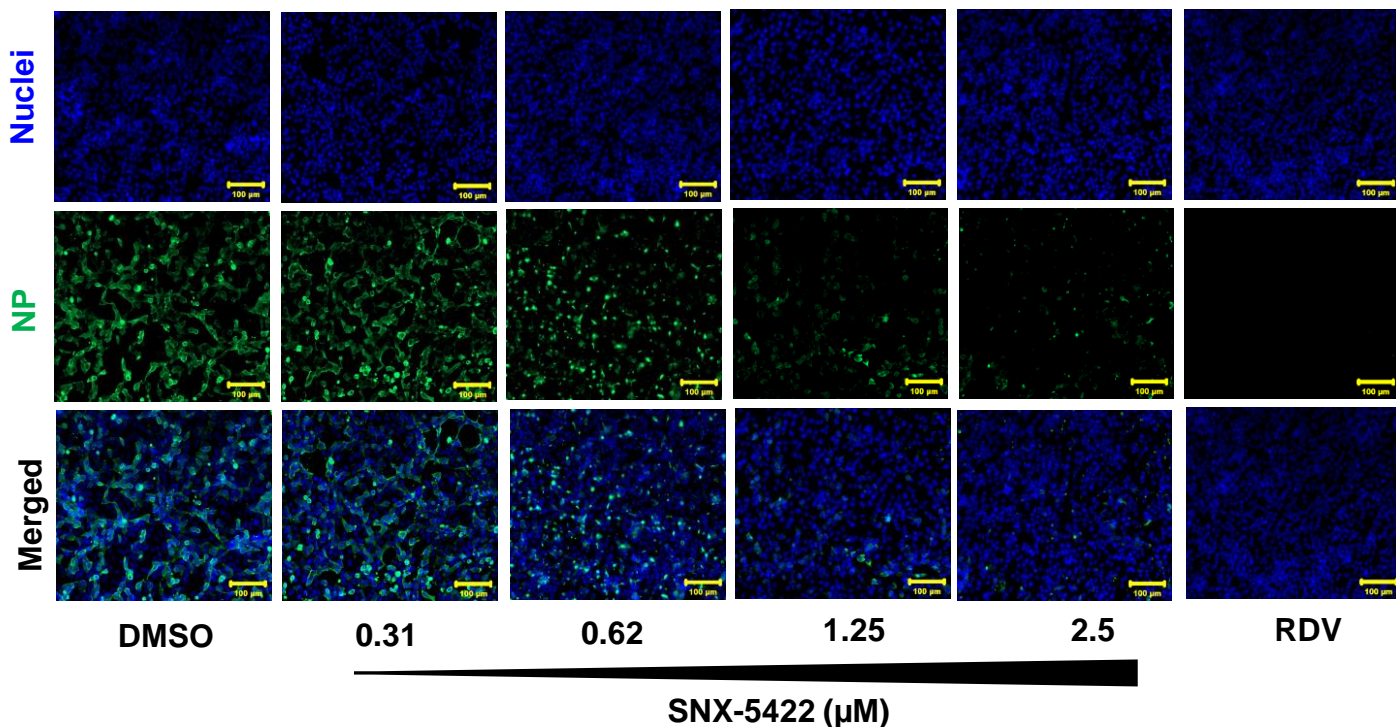
Cell-free SARS-CoV-2 RNA copies

C. Vero E6

D. Calu-3

G. Vero E6 cytotoxicity

Cell-free infectious SARS-CoV-2 titer
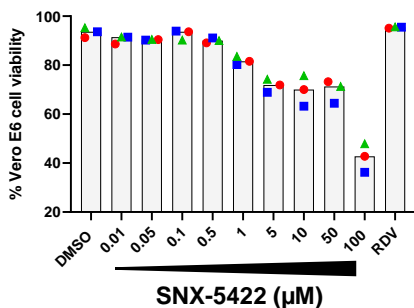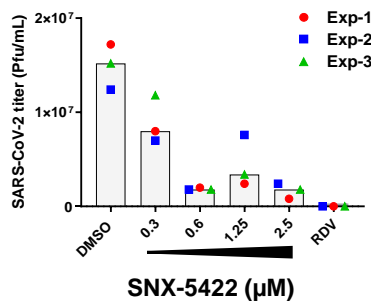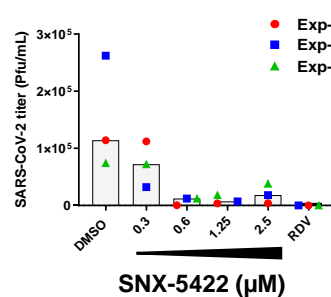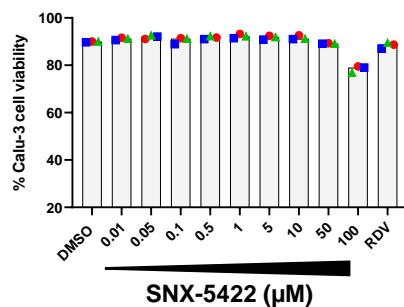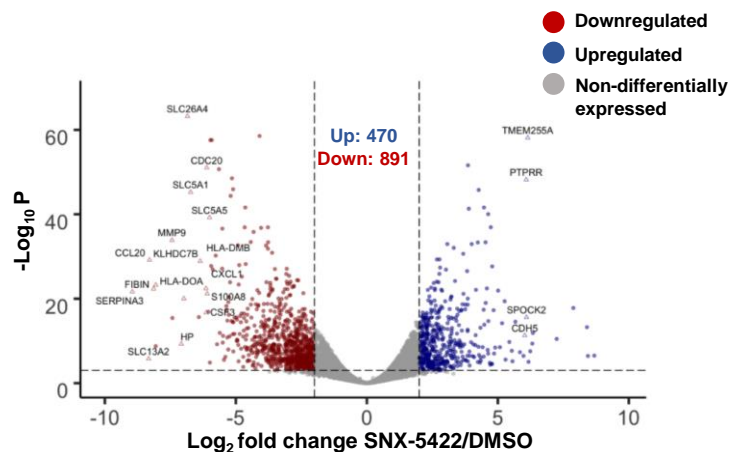
E. Vero E6

F. Calu-3

H. Calu-3 cytotoxicity

Figure 1. SNX-5422 potently suppresses SARS-CoV-2 replication at non-toxic concentrations.

Vero E6 and Calu-3 cells were infected with SARS-CoV-2 strain USA-WA1/2020 and treated with either 0.1% DMSO (drug-vehicle) or 0.31-2.5µM SNX-5422, or 5µM remdesivir (RDV). Both SNX-5422 and RDV were reconstituted in DMSO. After 48 hr post-infection (pi), **(A)** Vero cells were immunostained for SARS-CoV-2 nucleocapsid protein (NP) (green). Nuclei was counterstained (blue) prior to imaging. **(B)** Immunofluorescent images were quantified to evaluate proportions of SARS-CoV-2-NP+ cells. Each symbol and color represent an independent experiment and each data point represents an independent quantified image field. Medians of data points are reported as grey bars. Dotted line represents detection cut off, which is the mean+3 standard deviation (SD) of the percentage of NP+ cells in uninfected controls. Cell-free viral RNA in the supernatant of infected and treated **(C)** Vero-E6 and **(D)** Calu-3 cells were measured by qRT-PCR of the viral N gene. The infectious viral titers of the supernatant of **(E)** Vero E6 and **(F)** Calu-3 were determined by plaque assay. **(G)** Vero E6 and **(H)** Calu-3 cells were treated with either 0.1% DMSO (drug-vehicle) or 0.01-100µM SNX-5422, or 5µM RDV. After 48 hours, proportion of viable cells was evaluated by flow cytometry. Each symbol and color represent an independent experiment and medians of the data points are reported as grey bars.
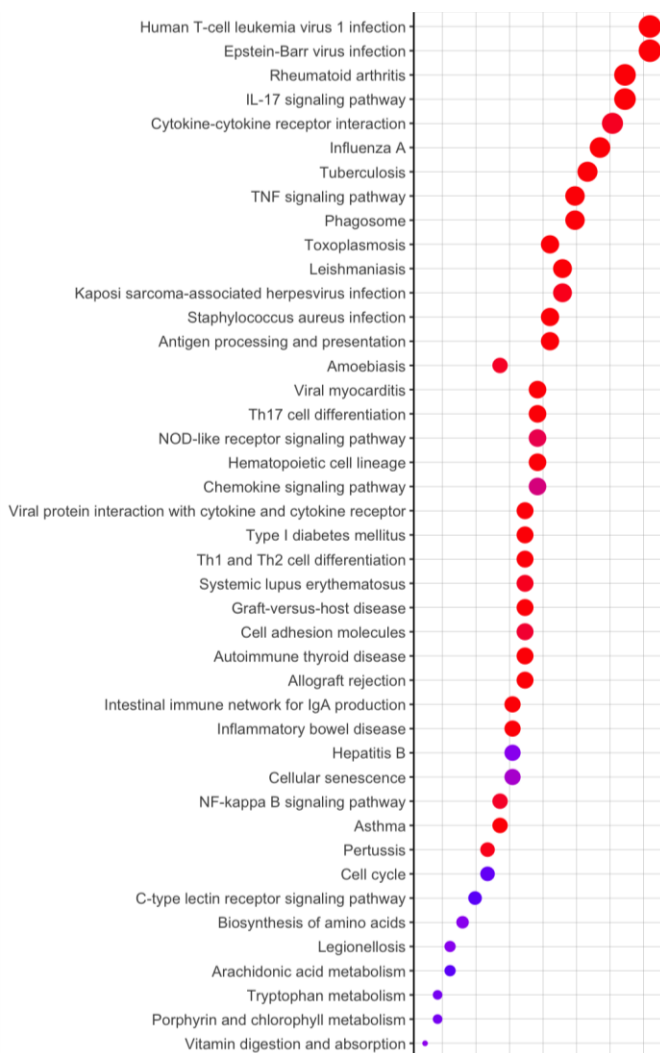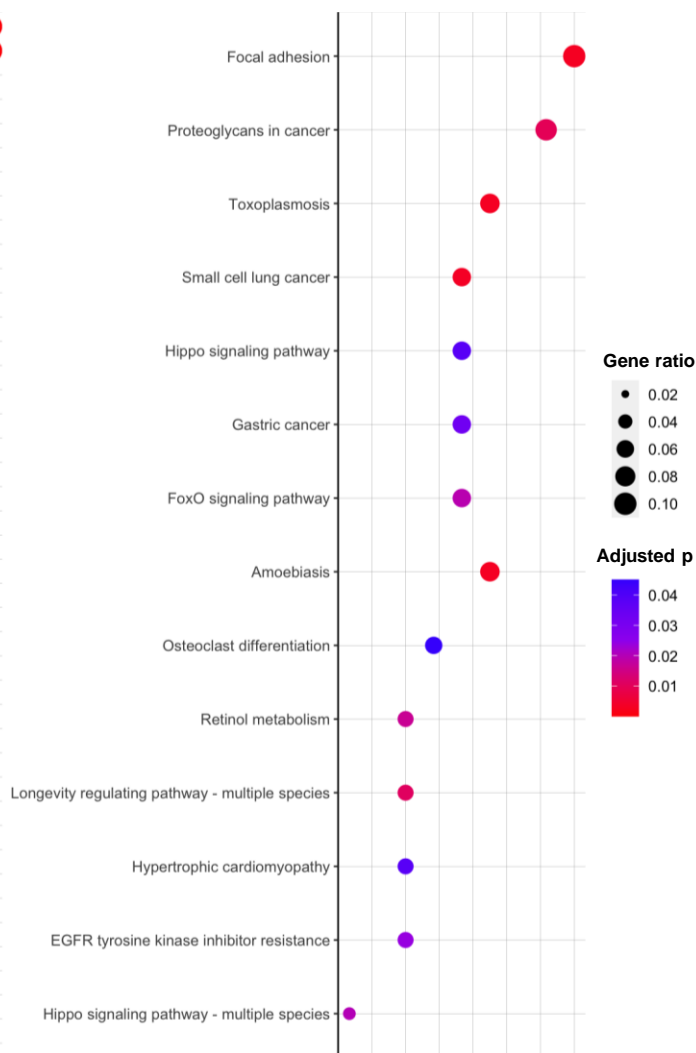
A. RNA-seq of human TBE cells

Apical side

Basolateral side

0.1% DMSO

SNX-5422

RNA extraction

Bulk RNA sequencing
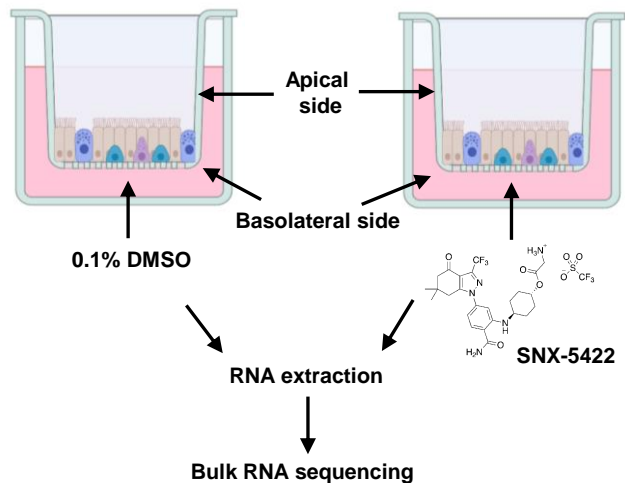
B. Genes differentially expressed upon SNX-5422 treatment

- Downregulated
- Upregulated
- Non-differentially expressed

Up: 470
Down: 891

$-Log_{10} P$

Log_2 fold change SNX-5422/DMSO

C. Downregulated KEGG pathways

D. Upregulated KEGG pathways

Gene ratio
- 0.02
- 0.04
- 0.06
- 0.08
- 0.10

Adjusted p
- 0.04
- 0.03
- 0.02
- 0.01
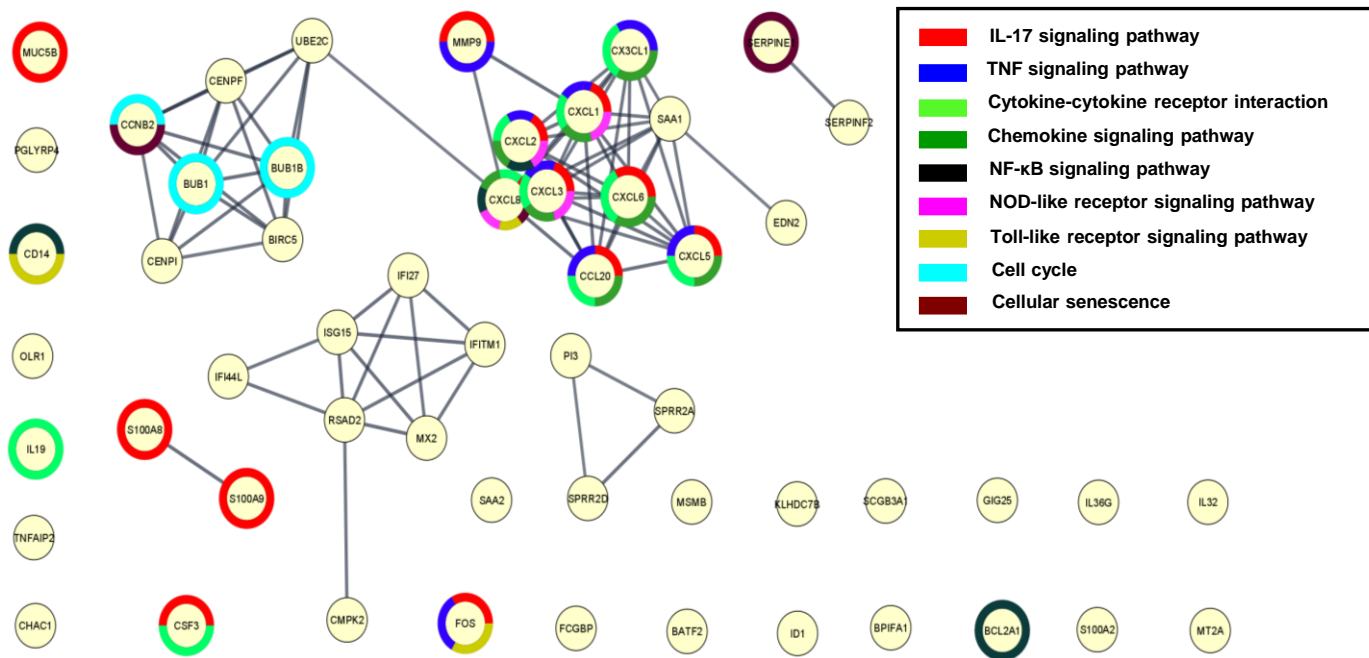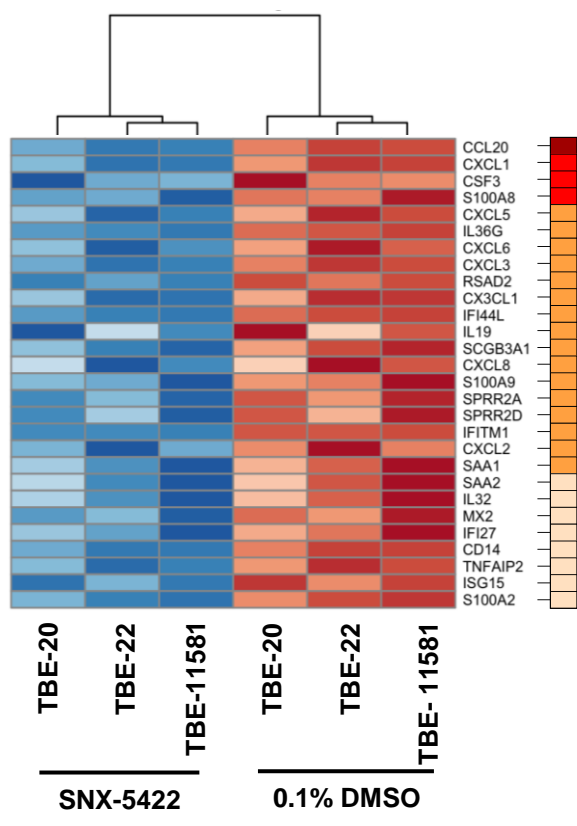
Figure 2. SNX-5422 treatment alters gene expression of human tracheobronchial epithelial (TBE) cells. (A) Schematic diagram illustrating treatment of human TBE cells. TBE cells from 3 independent healthy donors were cultured in air-liquid interface and treated with either 0.1% DMSO (drug-vehicle) or 1µM SNX-5422 reconstituted in DMSO, for 48hrs. RNA was then extracted from the cells and bulk RNA sequencing was performed. **(B)** Volcano plot demonstrating protein coding genes altered upon SNX-5422 treatment of human TBE cells. Red, blue and grey indicates downregulated, upregulated and non-differentially expressed genes, respectively. Differentially expressed genes (DEGs) were defined as protein coding genes with a Log_2 fold change >2 between the drug-treated and control groups and adjusted p value <0.001. Open symbols represent genes with Log_2 fold change >6 between the drug-treated and control groups. Cellular pathway overrepresentation analysis was performed with DEGs with a normalized average read count across donors and experimental conditions ≥300. **(C)** Downregulated and **(D)** Upregulated Kyoto Encyclopedia of Genes and Genomes (KEGG) pathways with an adjusted p value< 0.05 were reported. Dot size represented gene ratio and color schema represents adjusted p values.
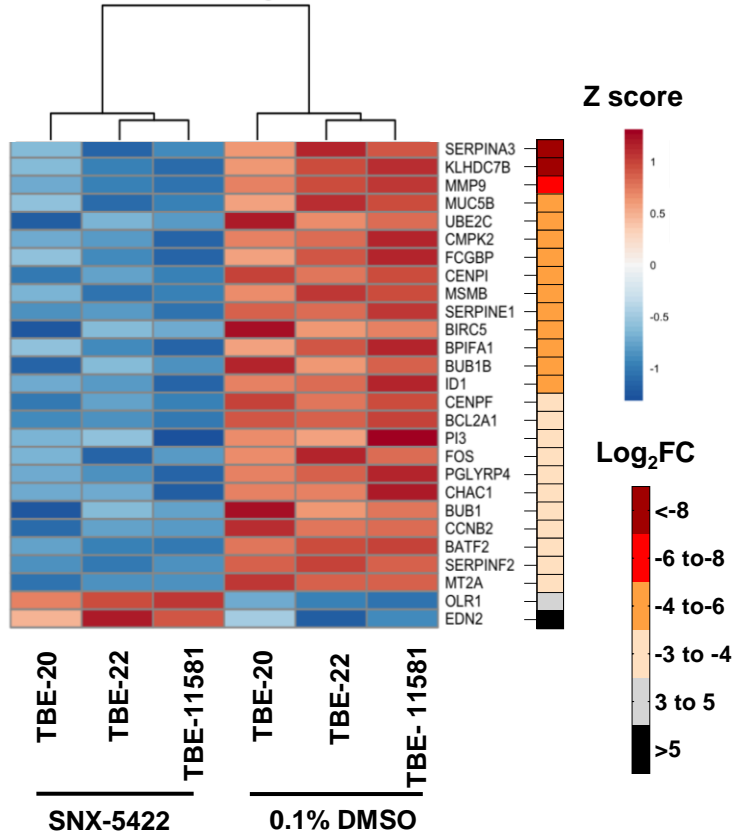
A. PPI network and functional enrichment of altered SARS-CoV-2 host factors

Legend:
- IL-17 signaling pathway (red)
- TNF signaling pathway (blue)
- Cytokine-cytokine receptor interaction (light green)
- Chemokine signaling pathway (dark green)
- NF-κB signaling pathway (black)
- NOD-like receptor signaling pathway (magenta)
- Toll-like receptor signaling pathway (yellow)
- Cell cycle (cyan)
- Cellular senescence (dark red)

B. SARS-CoV-2-mediated Hyperinflammation

C. SARS-CoV-2-mediated imbalanced host factors

Figure 3. SNX-5422 treatment targets cellular pathways and genes involved in SARS-CoV-2 replication and disease progression. (A) Protein-protein interaction (PPI) network and functional enrichment of genes altered by SNX-5422 that are involved in SARS-CoV-2 replication and COVID-19 progression. Each node represents a protein and interactions with confidence score >0.9 are presented. Heat maps of DEGs following SNX-5422 treatment of human TBE cells, that have been identified to be **(B)** associated with SARS-CoV-2-mediated hyperinflammation and **(C)** imbalanced upon viral infection. Red represents relative upregulation of gene expression and blue represents relative downregulation of gene expression. Gene expression counts were transformed, and Z score normalized for heat map generation. Donors were clustered with complete linkage. Genes are arranged based on fold changes, as indicated by the fold change key.

Table 1. Cell-specific SNX-5422 potency and selectivity

Cytotoxic Concentration (CC)				
	Cell line	**Assay**	**CC50[a] (µM)**	
	Vero E6	Cellular viability	91.97	
	Calu-3	Cellular viability	>100	
Inhibitory Concentration (IC)				
	Cell line	**Assay**	**IC50[b] (µM)**	**SI[c]**
	Vero E6	Cell-free SARS-CoV-2 RNA	0.2	459.85
		Cell-free infectious SARS-CoV-2 titer	0.38	242.03
		Intracellular SARS-CoV-2 N protein expression	2.3	39.99
	Calu-3	Cell-free SARS-CoV-2 RNA	0.2	>500
		Cell-free infectious SARS-CoV-2 titer	0.4	>250

[a]CC50: 50% cytotoxic concentration
[b]IC50: 50% inhibitory concentration
[c]SI: Selectivity index=CC50/IC50